Journal of chemical & engineering data

Article

pubs.acs.org/jced

Melting of Eutectic Mixtures in Silica and Carbon Nanopores

Małgorzata Sliwinska-Bartkowiak,*[,†] Monika Jazdzewska,[†] Marcin Trafas,[†] Milena Kaczmarek-Klinowska,[†,‡] and Keith E. Gubbins[§]

[†]Faculty of Physics, and [‡]Institute of Acoustics, Faculty of Physics, Adam Mickiewicz University, Umultowska 85, 61-614 Poznan, Poland

[§]Department of Chemical and Biomolecular Engineering, North Carolina State University, 911 Partners' Way, Raleigh, North Carolina 27695-7905, United States

ABSTRACT: We report experimental results for the melting of eutectic mixtures confined in nanoporous matrices. Dielectric relaxation spectroscopy and differential scanning calorimetry were used to determine the solid/liquid phase diagram of $C_6H_4Br_2/CCl_4$ mixtures confined in controlled pore glasses (CPG) with an average pore diameter of 7.5 nm, and C_6H_5Br/CCl_4 mixtures confined in activated carbon fibers (ACF) with a mean pore diameter of 1.4 nm. We find that the phase diagram of the confined mixtures are of the same type as that for the bulk mixture (eutectic). However, in the case of mixtures in carbon nanopores the solid/liquid coexistence lines are located at higher temperatures than for the bulk mixtures, whereas they are at lower temperatures than the bulk for mixtures confined in silica pores. These results are compared with those previously obtained for azeotropic mixtures in ACF. The results suggest that the melting temperatures, T_{mp}, of confined mixtures decrease relative to the bulk when the fluid−wall interactions are weaker than the fluid−fluid interaction (silica glasses), and increase in the case of fluid−wall interactions that are stronger than the fluid−fluid interaction (nanoporous carbons).

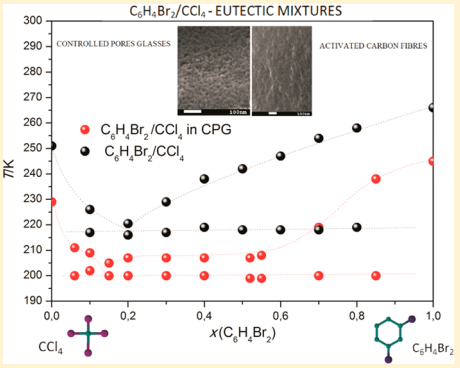

INTRODUCTION

Fluid or solid phases of nanoscale dimensions, when in contact with a solid surface or confined within a narrow pore, have thermodynamic properties that are often very different from those of the macroscopic bulk material. These confinement effects arise because of reduced dimensionality and strong interaction of the molecules in the nanophase with the confining walls. For several years special attention has been focused on the freezing and melting behavior of simple fluids confined in nanoporous materials, especially in mesoporous silicas.[1] It is known that for pore widths much larger than the diameter of the adsorbate molecules the shift in the melting points $\Delta T = T_{mbulk} - T_{mpore}$ can be connected with the pore width H using the Gibbs−Thomson equation.[2] Many experiments performed for pores larger than 6−7 nm showed a linear relation between the shift in the melting temperature and the inverse pore width, while for smaller pore diameters deviations from the Gibbs−Thomson equation have been observed.[2−5]

Recently a statistical mechanical analysis of such a nanophase (the adsorbate a, molecular diameter σ) was reported[5] confined within a porous material. From a corresponding states analysis of the partition function for pores of simple geometry (e.g., slit- or cylinder-shaped, with pore width H) it was shown that the principal system variables are the microscopic wetting parameter, α_w, and the dimensionless pore width $H^* = H/\sigma$. The wetting parameter is a measure of the relative strength of the adsorbate−wall and adsorbate−adsorbate interactions, and its definition emerges from the statistical mechanical analysis as

$$\alpha_w = \frac{\rho_s \varepsilon_{as} \sigma_{as}^2 \Delta}{\varepsilon_{aa}} \quad (1)$$

where ρ_s is the solid density in atoms per unit volume, σ_{as}, ε_{as}, and ε_{aa} are the usual size and energy parameters in the equation for the intermolecular potential energy, here taken to be the Lennard-Jones (12,6) model, and Δ is the interlayer spacing between layers of solid atoms in the substrate. The value of α_w depends strongly on the atomic density of the solid, as well as on the ratio of the two interaction well depths. This wetting parameter is closely correlated with the experimental contact angles for a wide range of liquids on various substrates.[6]

The melting and freezing behavior of fluids confined in pores of simple geometry can be understood in terms of two main system parameters, namely the pore width H and the wetting parameter α_w. It was shown[4] that adsorbents with $\alpha_w > 1$ can be considered to be "strongly attractive" (we expect an elevation in melting temperature relatively to the bulk melting point) while those with $\alpha_w < 1$ are "weakly attractive" (a depression in melting temperature relatively to the bulk is expected).

Very few studies of the melting of confined mixtures have been reported. Among these have been studies of confined molten salts[7,8] and colloidal mixtures.[9] Recently, molecular simulation and experimental studies of the confinement effect

Received: February 10, 2015
Accepted: September 4, 2015
Published: September 15, 2015

DOI: 10.1021/acs.jced.5b00131
J. Chem. Eng. Data 2015, 60, 3093−3100

on melting of azeotropic mixtures in carbon nanopores and silica glasses was reported.[10,11] The confined mixtures were found to have the same type of phase diagram as the bulk mixture,[12] but the melting temperature and characteristic concentrations were shifted relative to their bulk values.

In this paper, we present experimental results for eutectic mixtures in both silica and carbon nanopores. The solid−liquid phase diagram of the binary mixtures is presented for both the bulk and the confined systems to investigate the influence of confinement on both the melting temperature and the character of the solid−liquid phase diagram.

EXPERIMENTAL TECHNIQUES

We report experimental studies of the melting transition of two kinds of mixtures: $C_6H_4Br_2/CCl_4$ mixtures in controlled pores glasses (CPG), and C_6H_5Br/CCl_4 mixtures confined in activated carbon fibers (ACF). In our experiments we have used controlled pore glasses (CPG) (made by Corning Co., New Jersey) with an average pore diameter of 7.5 nm and a pore volume of 47 cc/g. The transmission electron microscopy (TEM) image of the CPG studied is presented in Figure 1a.

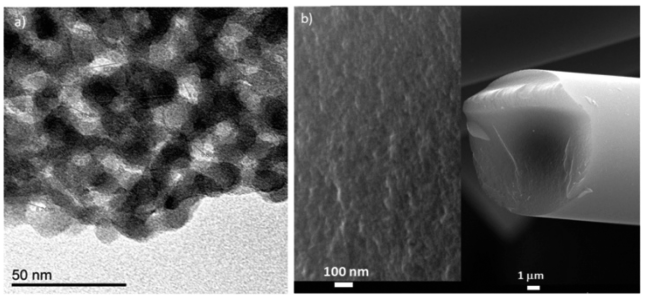

Figure 1. (a) TEM image of CPG silica glass, (b) SEM image of ACF.

The activated carbon fibers (ACF) (obtained from Prof. K. Kaneko Laboratory, Chiba University, Japan) have roughly slit-shaped pores with a mean pore width of 1.4 nm, and are built of nanocrystallites made up of defective graphene sheets (scanning electron microscopy (SEM) image in Figure 1b).

Before carrying out the experiments the porous materials were heated to about 400 K and kept under vacuum (10^{-3} Tr) for 4 days prior to the introduction of the liquids. Carbon tetrachloride, *m*-dibromobenzene and bromobenzene were twice distilled; after distillation the density of the liquids was measured using a DMA 38 density meter at 298 K temperature and at normal pressure. The characterization of the liquids used is presented in Table 1.

The melting of mixtures confined in CPG and ACF was determined using dielectric relaxation spectroscopy (DRS) and differential scanning calorimetry (DSC) methods.[13] Dielectric measurements were performed using a parallel plate capacitor.[13] The capacitance C and the tangent loss of the samples were measured at different temperatures T and frequencies ω using a Solartron 1260 gain impedance analyzer, in the frequency range 1 Hz to 1 MHz. The sample was introduced between the capacitor plates as a suspension of nanoporous particles filled with the mixture, so that the permittivity measurements have contributions from both the bulk and confined mixtures. For dipolar liquids the melting of a solid phase is accompanied by a rapid increase of the real part of the permittivity, due to the increase of the dipolar polarization in the liquid state.[11] The DSC method was applied to determine the phase transition temperatures of the confined systems by measuring the heat released in the melting process. The instrument used was a DSC Q2000 calorimeter (TA Instruments in Departmental Laboratory of Structural Research in Faculty of Physics). Temperature scanning rates of 5 K/min to 10 K/min in the range between 110 K and 330 K were used in the experiments.

EXPERIMENTAL RESULTS

The melting of mixtures of $C_6H_4Br_2(2)/CCl_4(1)$ confined in CPG, and also of $C_6H_5Br(2)/CCl_4(1)$ confined in ACF, as well as in the bulk phase, was determined by monitoring temperature changes in the dielectric permittivity, ε, that occur at the transition from the solid to liquid phases. The melting of dipolar liquids such as dibromobenzene is accompanied by a rapid increase in ε' (the real part of the dielectric permittivity). Below the melting temperature, the rotational phase ceases to exist, and ε' is almost equal to n^2 (n is the refractive index) and it is only related to the deformation polarization; for the liquid phase a maximum value, ε'_m, of the permittivity is observed due to the dipolar polarization of the liquid. By measuring the functions $\varepsilon'(T)$ or $C(T)$ (C is the electric capacity of the system) we can observe the values of ε'_m and ε'_s (permittivity in the solid state) in the vicinity of the melting points, and thus determine the values of the melting temperatures of the systems. From these measurements we construct the phase diagram of the system on the $(T,x_2)-p$ plane (x_2 is the mole fraction of the dipolar liquid in the mixture). From the dielectric data we can also determine the relaxation processes related to molecular motion in particular phases.

The electric capacity C of $C_6H_4Br_2/CCl_4$ mixtures was measured in the whole concentration range and over a wide range of temperatures during the melting process. Figure 2a,b,c shows C versus temperature for $C_6H_4Br_2/CCl_4$ bulk mixtures of various molar compositions. The transition from the solid state (characterized by the minimum values of C, which is almost temperature-independent) to the liquid state is observed over a wide temperature range, which changes with increasing mole fraction of *m*-dibromobenzene. For concentration $x_2 \approx 0.2$ a sharp increase of $C(T)$, typical of pure liquids is observed. For $x_2 \geq 0.2$, the temperature range of the phase transitions regions is found to broaden. Assuming that the melting process starts at temperature T_2, the temperature of the change in the monotonic character of $C(T)$, and taking T_1 as the temperature

Table 1. Chemical Sample Table. Density ρ at 298 K, and Pressure p = 0.1 MPa

chemical name	source	mole fraction purity	purification method	density [g/cm^3]	analysis method
carbon tetrachloride	POCH S.A.	0.99	twice distilled	1.594	density
m-dibromobenzene	Sigma-Aldrich	0.97	twice distilled	1.952	density
bromobenzene	Sigma-Aldrich	0.99	twice distilled	1.491	density

Standard uncertainties u are $u(\rho)$ = 0.005 g/cm^3, $u(T)$ = 0.3 K and $u(p)$ = 5 kPa.

DOI: 10.1021/acs.jced.5b00131
J. Chem. Eng. Data 2015, 60, 3093−3100

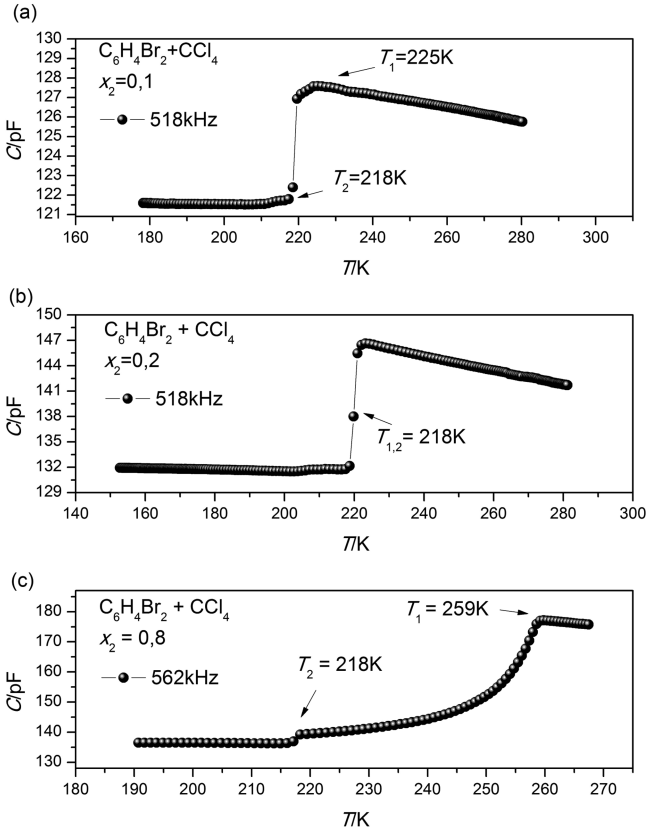

Figure 2. Capacity C as a function of temperature T for bulk $C_6H_4Br_2(2)/CCl_4(1)$ mixtures for (a) $x_2 = 0.1$; (b) $x_2 = 0.2$; (c) $x_2 = 0.8$. T_2 corresponds to the melting process; T_1 is the temperature at which the transition into the homogeneous mixture is complete.

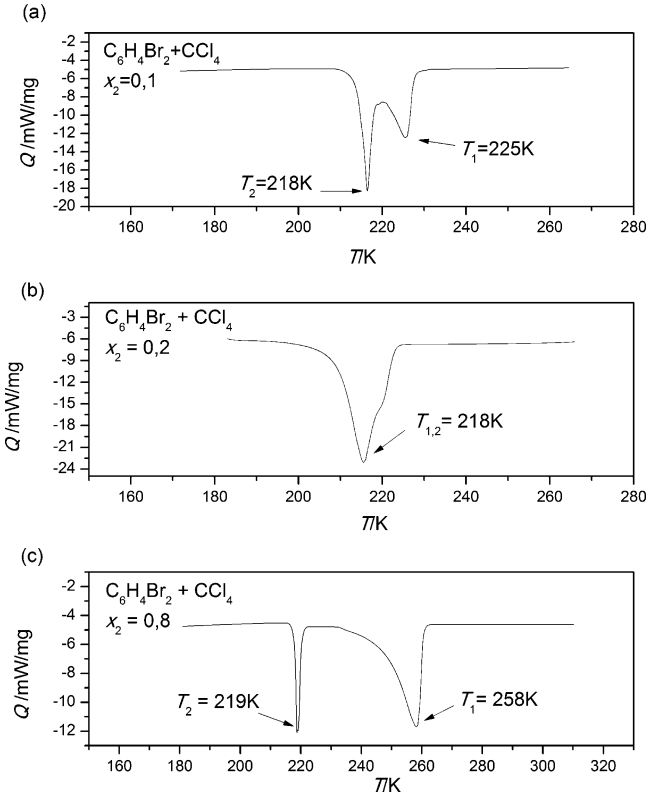

Figure 3. DSC scan for bulk $C_6H_4Br_2/CCl_4$ mixtures for (a) $x_2 = 0.1$ composition; (b) $x_2 = 0.2$; (c) $x_2 = 0.8$.

Table 2. Melting Temperature T for a Bulk $C_6H_4Br_2/CCl_4$ Mixtures for Different Dibromobenzene Mole Fraction (from 0 to 1)[a]

x_2	T_2/K	T_1/K
0.00		252.4
0.10	218.0	225.0
0.20	218.0	220.5
0.30	218.3	229.7
0.40	218.8	237.8
0.50	218.1	242.7
0.60	218.2	247.2
0.70	218.0	254.1
0.80	218.0	259.0
1.00		266.0

[a] T_2 corresponds to the beginning of the melting process while T_1 is the temperature at which the transition into the homogeneous liquid state is complete. Mole fraction, x_2; temperature, T, and pressure p = 0.1 MPa. Standard uncertainties u are $u(T)$ = 0.7 K, $u(x_2)$ = 0.01 and $u(p)$ = 5 kPa.

at which the transition into the homogeneous liquid state is complete, we can construct the phase diagram $(T,x_2)-p$ of the mixture. Investigation of the dielectric relaxation processes versus temperature related to molecular motion in particular phases is discussed below.

DSC measurements for bulk phase $C_6H_4Br_2/CCl_4$ mixtures were also performed, using a heating rate in the range 0.5 K/min to 10 K/min. The results obtained were fully reproduceble. The DSC scans are shown in Figure 3a,b,c. Two DSC peaks are observed, which correspond to the transition temperatures T_1 and T_2 obtained from the dielectric method. In Figure 3b an irregular DSC peak is observed for concentration $x_2 \approx 0.2$, showing a very narrow temperature range of the phase transitions, similar to that observed in Figure 2b.

In Table 2 the values of temperatures of solidus cuve (T_1) and liquidus curve (T_2) versus concentration x_2 obtained for the bulk $C_6H_4Br_2/CCl_4$ mixtures using dielectric method are presented.

In Figure 4 the bulk phase diagram for the $C_6H_4Br_2/CCl_4$ mixture is shown; the diagram is typical for a simple eutectic mixture. The line AEB is the liquidus line, constructed from the temperature T_1 at which the system is in the liquid phase in equilibrium with a solid phase. The line CD is a solidus line, obtained from the temperature T_2; below this temperature the entire system is in the solid state. At the eutectic point E the solid constituents m-$C_6H_4Br_2$ and CCl_4 are in equilibrium with the liquid mixture of composition $x_2^E \sim 0.2$. The melting points of the two components of the $C_6H_4Br_2/CCl_4$ mixtures are different ($C_6H_4Br_2$ – 266 K and CCl_4 – 250.4K), so the eutectic concentration is shifted toward the component having the lower melting temperature. The capacitance curve $C(T)$ as a function of the temperature was also studied for the $C_6H_4Br_2/CCl_4$ mixture placed in CPG. Because the sample was introduced as a suspension of CPG particles in bulk mixtures, the signals we observed were from both the bulk and confined system.

In Figure 5 a,b we present the melting transition for bulk $C_6H_4Br_2$ as determined by both DRS and DSC. The results show a sudden increase in $C(T)$ at the melting temperature 266 K (Figure 5a) and an endothermic peak in the DSC scan at 266 K, both related to the melting transition of m-$C_6H_4Br_2$ (Figure

DOI: 10.1021/acs.jced.5b00131
J. Chem. Eng. Data 2015, 60, 3093−3100

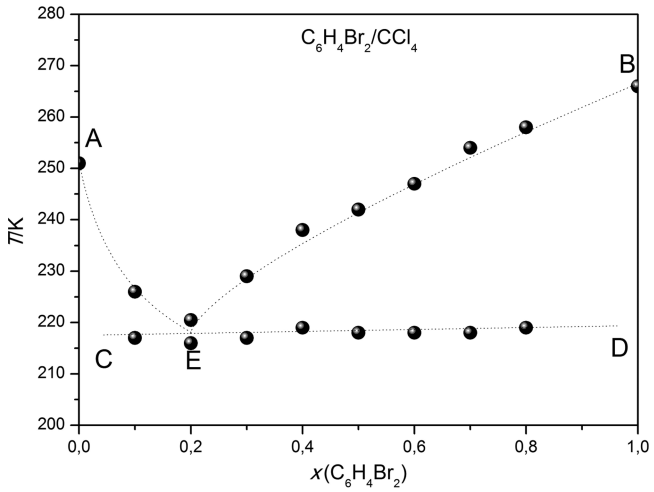

Figure 4. Solid−liquid phase diagram (T,x_2) for C_6H_4Br/CCl_4 bulk mixtures.

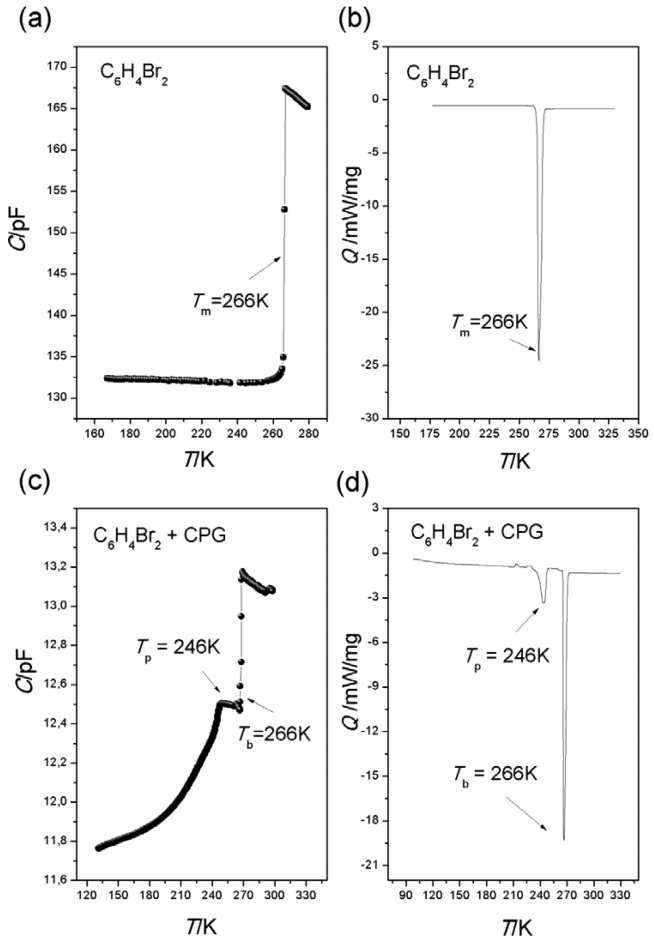

Figure 5. (a) Capacitance C versus temperature for bulk $C_6H_4Br_2$; (b) DSC scan for bulk $C_6H_4Br_2$; (c) capacitance C versus temperature for $C_6H_4Br_2$ in CPG; (d) DSC scan for $C_6H_4Br_2$ in CPG with pores of average diameter 7.5 nm.

5b). In Figure 5c and 5d the capacity curve $C(T)$ and DSC scan for m-$C_6H_4Br_2$ in CPG of diameter of 7.5 nm are presented. As seen from Figure 5c, the $C(T)$ function exhibits two sharp changes: at 246 K, which is attributed to the melting in pores, and at 266 K resulting from the melting of bulk m-$C_6H_4Br_2$. The analysis of the DSC scan (Figure 5d) shows also the melting transitions at 246 and 266 K, which are attributed to the melting in pores and the bulk m-$C_6H_4Br_2$, respectively. We observed a decrease of the melting temperature of $C_6H_4Br_2$ in CPG pores of about 20 K relative to the bulk phase. For $C_6H_4Br_2/CCl_4$ mixtures confined in CPG (Figure 6 a,b,c), T_1 corresponds to the temperature at the liquidus line, while T_2 is the temperature at the solidus line of the bulk mixture. The changes observed in the $C(T)$ function at the lower temperatures T_{1p} and T_{2p} are attributed to the melting in CPG, and correspond to the liquidus and solidus lines for the $C_6H_4Br_2/CCl_4$ mixture confined in CPG.

In Figure 6 panels d and e the DSC scan for the melting of the $C_6H_4Br_2/CCl_4$ mixtures of 0.3 and 0.4 mole fraction confined in CPG is presented. We observe four DSC peaks related with the transition temperatures: T_1, T_2, T_{1p}, and T_{2p}. These transition temperatures are also observed by the dielectric method. The signals at temperatures T_1 and T_2 correspond to the melting of the bulk mixture, while the two DSC peaks at T_{1p} and T_{2p} are attributed to the melting in pores. The phase transition temperatures corresponding to the solidus/liquidus lines estimated by the DSC method were consistent with those obtained from the analysis of the $C(T)$ function for this system.

The temperatures of solidus line T_{2p} and liquidus line T_{1p} for $C_6H_4Br_2/CCl_4$ mixtures confined in CPG for various concentrations of m-$C_6H_4Br_2$ obtained on the basis of dielectric measurements are presented in Table 3.

The phase diagram for the $C_6H_4Br_2/CCl_4$ mixtures confined in CPG compared with its bulk phase diagram (Figure 3) constructed on the basis of our dielectric and DSC measurements is presented in Figure 7.

As seen from Figure 7, the phase diagram of the confined mixture is of the same type as for the bulk mixture, that is, that for a eutectic mixture. The melting point of CCl_4 confined in CPG with pores of 7.5 nm diameter is 229 K,[14] while that for $C_6H_4Br_2$ in CPG is 246 K. These values of the melting temperatures in pores suggest that the eutectic composition x_{2p}^{E} in pores should be shifted toward the component having the lower melting temperature, CCl_4. Our results show x_{2p}^{E} = 0.15 in the pores, lower than the bulk eutectic composition, x_2^{E} = 0.2. It is also seen that the melting point of the confined mixture is lower than that of the bulk mixture (the eutectic temperatures, T_E, are about 200 K and 220 K for the confined and bulk mixtures, respectively). The depression of the melting temperature of the confined systems relative to the bulk is typical of systems for which the ratio of the fluid/wall to the fluid/fluid interaction is considerably lower than 1. For liquids having a wettability parameter α_w much larger than 1, an increase of the melting temperature is generally observed, as is often the case for liquids adsorbed on nanoporous carbons, due to the high atomic density of the pore walls.[4]

The melting of C_6H_5Br/CCl_4 mixtures confined in ACF pores of mean diameter 1.4 nm was determined using the dielectric method. The C_6H_5Br/CCl_4 bulk mixture also forms an eutectic system,[12] with the eutectic concentration x_2^{E} = 0.48 and eutectic temperature T_E = 210 K, as shown in Figure 8.

The melting temperatures of the two components are similar (bromobenzene 244 K and carbon tetrachloride 250.4 K) and the eutectic concentration x_2^{E} is close to 0.5. In Figure 9 the capacity C is shown versus T for C_6H_5Br in ACF. As seen from Figure 9, the melting temperature of bulk C_6H_5Br is observed as a sudden increase of $C(T)$ at a temperature 244 K; at 271 K

DOI: 10.1021/acs.jced.5b00131
J. Chem. Eng. Data 2015, 60, 3093−3100

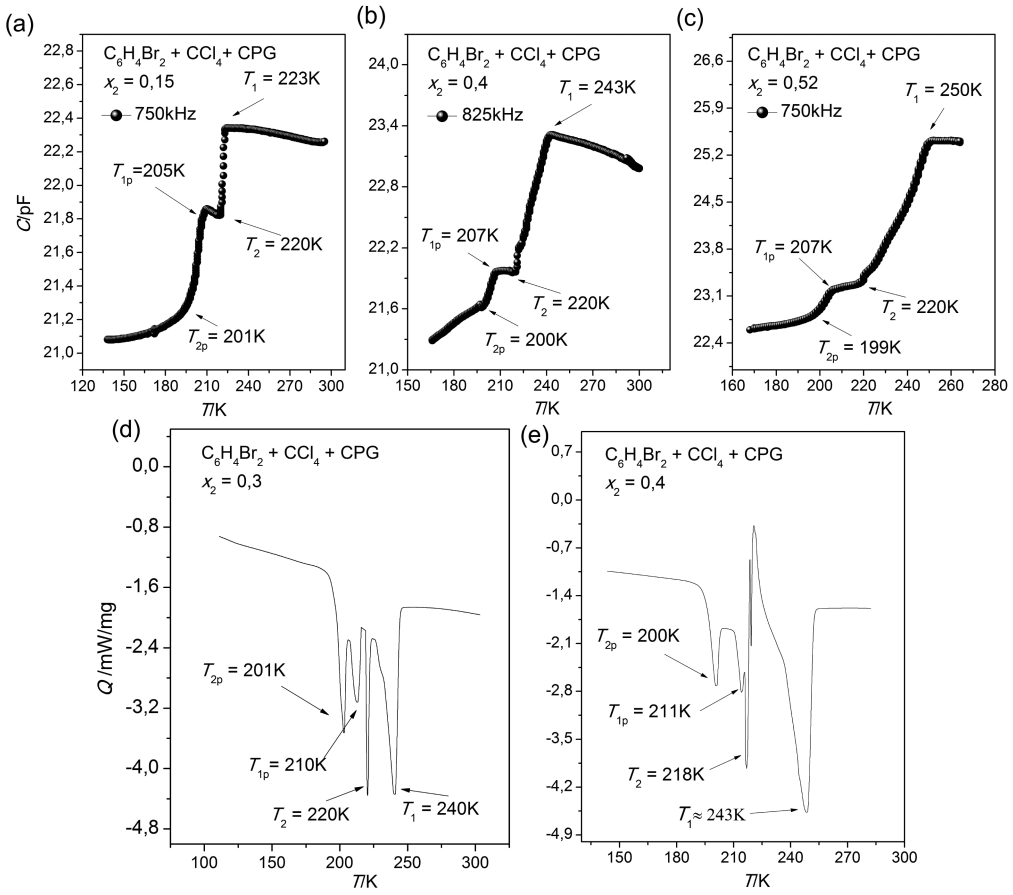

Figure 6. Capacity C as a function of temperature T for $C_6H_4Br_2/CCl_4$ mixtures of different concentrations confined in CPG: (a) $x_2 = 0.15$, (b) $x_2 = 0.4$, and (c) $x_2 = 0.52$; DSC scan for $C_6H_4Br_2/CCl_4$ mixtures confined in CPG of (d) $x_2 = 0.3$ and (e) $x_2 = 0.4$.

Table 3. Melting Temperature T for $C_6H_4Br_2/CCl_4$ Mixtures Confined in CPG for Different Dibromobenzene Mole Fraction (from 0 to 1)[a]

x_2	T_{2p}/K	T_{1p}/K
0.00		229.0
0.10	201.9	209.0
0.15	201.0	205.0
0.20	200.1	207.2
0.30	201.0	208.0
0.40	200.0	207.0
0.52	199.0	207.0
0.55	199.1	208.1
0.70	200.1	218.9
0.85	200.0	238.2
1.00		246.0

[a] T_2 corresponds to the beginning of the melting process while T_1 is the temperature at which the transition into the homogeneous liquid state is complete. Mole fraction, x_2; temperature, T; and pressure, p = 0.1 MPa. Standard uncertainties u are $u(T) = 0.7$ K, $u(x_2) = 0.01$ and $u(p) = 5$ kPa.

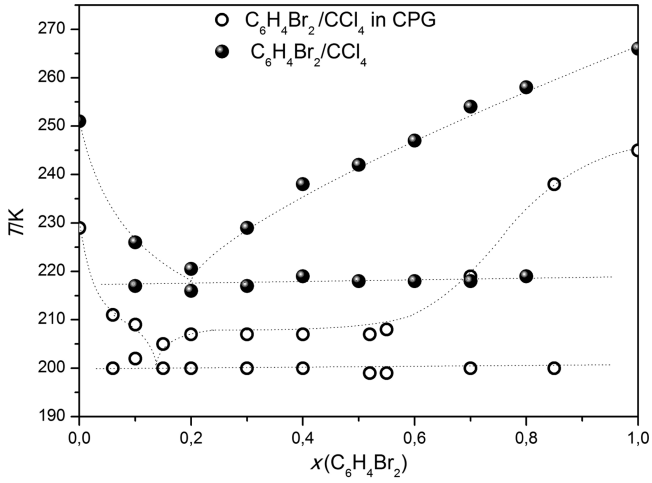

Figure 7. Solid−liquid phase diagrams (T,x_2) for $C_6H_4Br_2(2)/CCl_4(1)$ bulk mixtures (solid circles) and mixtures confined in CPG (open circles).

the next phase transition behavior is observed as an increase in $C(T)$, which can be attributed to the melting in pores. The melting temperature of CCl_4 confined in ACF pores of diameter of 1.4 nm is 298 K.[15]

In Figure 10 panels a, b, and c, the $C(T)$ functions for C_6H_5Br/CCl_4 mixtures placed in ACF of various compositions are presented. At temperatures T_1 and T_2 in Figure 10, we observe changes of the $C(T)$ function related to phase transitions of the bulk C_6H_5Br/CCl_4 mixtures, typical for liquidus and solidus lines, respectively. The sudden changes observed for $C(T)$ at the high temperatures T_{1p} and T_{2p} are related to the melting in ACF pores.

The values of temperatures of the solidus T_{2p} and liquidus T_{1p} line for various concentrations of C_6H_5Br for C_6H_5Br/CCl_4

DOI: 10.1021/acs.jced.5b00131
J. Chem. Eng. Data 2015, 60, 3093−3100

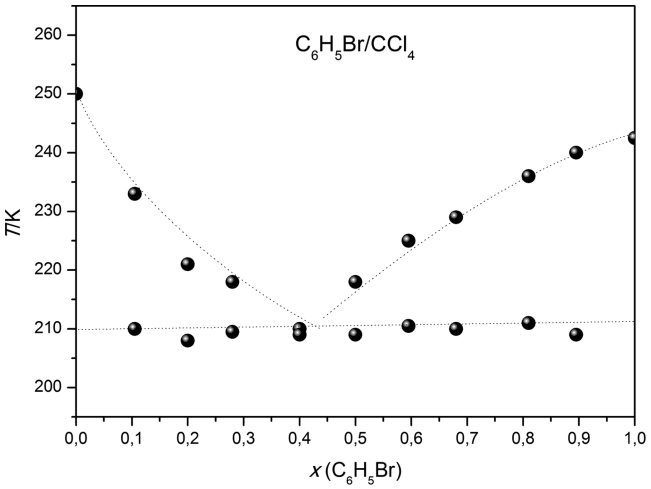

Figure 8. Solid−liquid phase diagrams (T,x_2) for C_6H_5Br/CCl_4 bulk mixtures; x_2 is the bromobenzene mole fraction. Data are taken from ref 12.

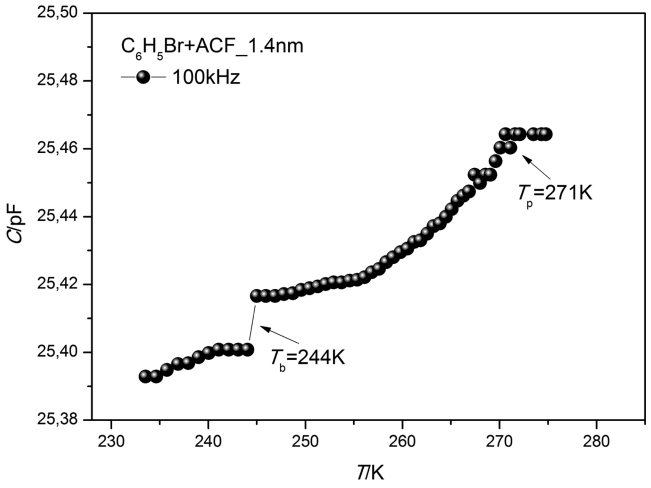

Figure 9. Capacity C versus temperature for C_6H_5Br in ACF pores of diameter 1.4 nm.

mixtures confined in ACF obtained from dielectric measurements are presented in Table 4.

Table 4. Melting Temperature T for C_6H_5Br/CCl_4 Mixtures Confined in ACF for Different Bromobenzene Mole Fraction (from 0 to 1)[a]

x_2	T_{2p}/K	T_{1p}/K
0.00		298.0
0.10	247.9	273.0
0.20	249.9	265.1
0.30	248.0	263.0
0.40	248.0	261.2
0.50	240.2	259.9
0.55	249.1	260.0
0.60	248.0	248.0
0.70	241.0	261.0
0.80	249.8	270.1
1.00		271.0

[a] T_2 corresponds to the beginning of the melting process while T_1 is the temperature at which the transition into the homogeneous liquid state is complete. Mole fraction, x_2; temperature, T; and pressure, p = 0.1 MPa. Standard uncertainties u are $u(T)$ = 0.8 K, $u(x_2)$ = 0.01 and $u(p)$ = 5 kPa.

The phase diagram for the C_6H_5Br/CCl_4 mixtures confined in ACF, constructed on the basis of dielectric measurements, is compared with the diagram for bulk mixtures (Figure 8), and is presented in Figure 11. As follows from Figure 11 the type of phase diagram for C_6H_5Br/CCl_4 mixtures placed in ACF is also eutectic, similar to that for the bulk mixture. The melting point of CCl_4 placed in ACF is higher than the melting temperature of C_6H_5Br confined in ACF, so we can expect that the eutectic composition x_{2p}^{E} in pores will be shifted toward the component with the lower melting point, that is, toward C_6H_5Br. Our results show that x_{2p}^{E} = 0.6, which is larger than the bulk eutectic concentration, x_2^{E} = 0.48. As shown in Figure 11, the melting temperature of the confined mixture is higher than that of the bulk (the T_E values are 245 and 210 K for the confined and bulk mixtures, respectively).

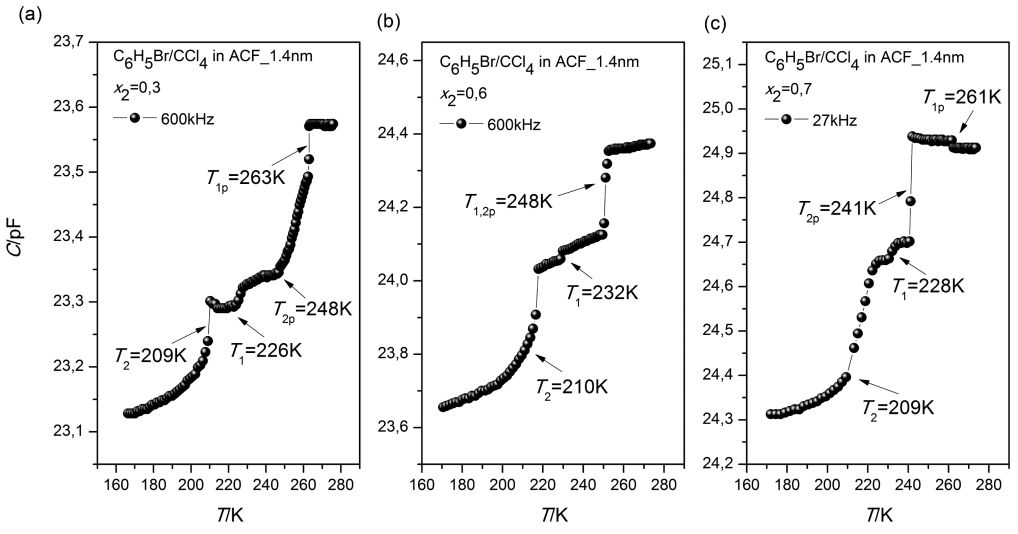

Figure 10. Electric capacity $C(T)$ for C_6H_5Br/CCl_4 mixtures confined in ACF of mean pore diameter 1.4 nm for various compositions: (a) x_2 = 0.3, (b) x_2 = 0.6, and (c) x_2 = 0.7.

DOI: 10.1021/acs.jced.5b00131
J. Chem. Eng. Data 2015, 60, 3093−3100

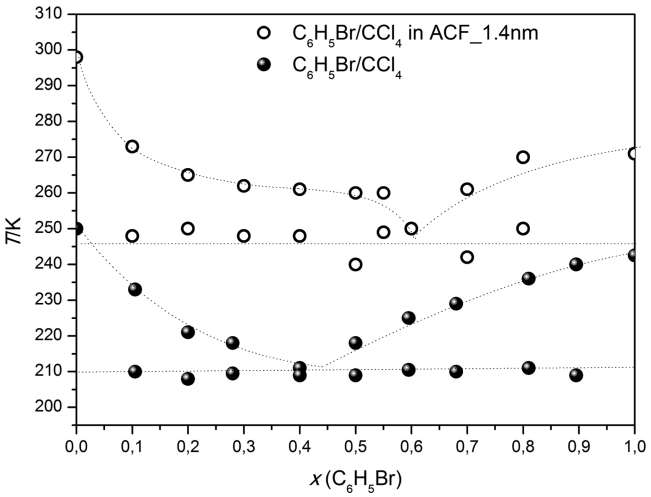

Figure 11. Solid−liquid phase diagrams (T,x_2) for C_6H_5Br/CCl_4 bulk mixtures (solid circles) and mixtures confined in ACF (open circles).

It was found that for the system $C_6H_4Br_2/CCl_4$ mixtures placed in CPG the melting temperatures are lower than those for the bulk mixture. By contrast, the C_6H_5Br/CCl_4 mixture confined in ACF exhibits an elevation of the melting temperature relative to that of the bulk mixture. This result can be explained on the basis of the value of the wetting parameter, α_w, for fluids confined in nanopores. The value of α_w eq 1 depends strongly on the atomic density of the solid, and on the interlayer spacing and fluid−wall diameter. For carbon this density is 114 nm^{-2}, but for silica[16] it is about 57 nm^{-2}. Also the interlayer spacing Δ is smaller for silica than for carbon.[16] As a result, the value of α_w for a given fluid interacting with carbon is higher than that the same fluid on silica. Both molecular simulation and experimental studies of freezing/melting of simple fluids in well characterized pores indicate that large α_w values lead to an elevation in the melting temperature, while the reverse is true for small α_w, the threshold value of α_w being close to unity.[4,16−18] Thus, we can expect an increase in the melting temperature for the mixtures placed in ACF pores and a decrease of melting temperature for the mixtures in silica pores, as has been observed experimentally here. An elevation of the melting temperature relative to that for the bulk mixture has also been observed for the azeotropic mixture, CCl_4/C_6H_{12}, confined in ACF pores.[9,10] This system also exhibits a large value of α_w.

CONCLUSIONS

We have reported the results of experiments on the melting of eutectic mixtures confined in carbon and silica nanopores. The solid−liquid phase diagram of $C_6H_4Br_2/CCl_4$ mixtures confined in controlled pore glass with an average pore size of H = 7.5 nm, and of C_6H_5Br/CCl_4 mixtures confined in activated carbon fibers having a mean pore size of H = 1.4 nm were constructed using the results of dielectric relaxation spectroscopy and differential scanning calorimetry measurements. We observed that the type of phase diagrams for the confined mixtures were the same as those for the bulk mixtures, namely eutectic. It was also observed that the eutectic concentrations for both systems were shifted toward the component having the lower melting point in the pores, that is toward the component having the smaller wetting parameter, α_w. These effects were also observed in previous work for confined azeotropic mixtures.[10,11]

For the $C_6H_4Br_2/CCl_4$ mixtures confined in CPG a depression of the melting temperature relative to that of the bulk mixture was observed, whereas for C_6H_5Br/CCl_4 mixtures placed in ACF an elevation of the melting point occurred. In conclusion, we note that the effect of confinement in carbon (ACF) and silica (CPG) pore on the melting temperatures of mixtures can be understood in terms of the wetting parameters of these systems.

AUTHOR INFORMATION

Corresponding Author

*E-mail: msb@amu.edu.pl.

Funding

We thank the National Center of Science of Poland for financial support under Grant DEC-2013/09/B/ST4/03711. K.E.G. thanks the U.S. National Science Foundation under Grant No. CBET 1160151 for support of this research.

Notes

The authors declare no competing financial interest.

ACKNOWLEDGMENTS

We would like to thank M.Sc. A. Sterczyńska for TEM and SEM images of the porous materials used here, which were obtained in the NanoBioMedical Centre in Poznan.

REFERENCES

(1) Gelb, L.; Radhakrishnan, R.; Gubbins, K. E.; Sliwińska-Bartkowiak, M. Phase Separation in Confined Systems. *Rep. Prog. Phys.* **1999**, *62*, 1573−1659.

(2) Alba-Simionesco, C.; Coasne, B.; Dosseh, G.; Dudziak, G.; Gubbins, K. E.; Radhakrishnan, R.; Sliwinska-Bartkowiak, M. Effects of Confinement on Freezing and Melting. *J. Phys.: Condens. Matter* **2006**, *18*, R15−R68.

(3) Radhakrishnan, R.; Gubbins, K. E.; Sliwinska-Bartkowiak, M. Effect of the fluid-wall interaction on freezing of confined fluids: Toward the development of a global phase diagram. *J. Chem. Phys.* **2000**, *112*, 11048−11057.

(4) Radhakrishnan, R.; Gubbins, K. E.; Sliwinska-Bartkowiak, M. Global phase diagrams for freezing in porous media. *J. Chem. Phys.* **2002**, *116*, 1147−1155.

(5) Gubbins, K. E.; Long, Y.; Sliwinska-Bartkowiak, M. Thermodynamics of confined nano- phases. *J. Chem. Thermodyn.* **2014**, *74*, 169−183.

(6) Sliwińska-Bartkowiak, M.; Sterczynska, A.; Long, Y.; Gubbins, K. E. Influence of microroughness on the wetting properties of nanoporous silica matrices. *Mol. Phys.* **2014**, *112*, 2365−2371.

(7) Meyer, R. R.; Sloan, J.; Dunin-Borkowski, R. E.; Kirkland, A. I.; Novotny, M. C.; Bailey, S. R.; Hutchinson, J. L.; Greene, M. L. H. Discrete Atom Imaging of One Dimensional Crystals Formed Within Single-Walled Carbon Nanotubes. *Science* **2000**, *289*, 1324−1326.

(8) Wilson, M. The Formation of Low-Dimensional Ionic Crystallites in Carbon Nanotubes. *J. Chem. Phys.* **2002**, *116*, 3027−3041.

(9) Cui, B.; Lin, B.; Rice, S. A. Structure and phase transitions in confined binary colloid mixtures. *J. Chem. Phys.* **2003**, *119*, 2386−2398.

(10) Coasne, B.; Czwartos, J.; Gubbins, K. E.; Hung, F. R.; Sliwinska-Bartkowiak, M. Freezing and Melting in Binary Mixtures Confined in a Nanopore. *Mol. Phys.* **2004**, *102*, 2149−2163.

(11) Coasne, B.; Czwartos, J.; Sliwińska-Bartkowiak, M.; Gubbins, K. E. Effect of Pressure on the Freezing of Pure Fluids and Mixtures Confined in Nanopores. *J. Phys. Chem. B* **2009**, *113*, 13874−13881.

(12) Czwartos, J.; Coasne, B.; Sliwińska-Bartkowiak, M.; Gubbins, K. E. Melting of mixtures in silica nanopores. *Pure Appl. Chem.* **2009**, *81*, 1953−1959.

(13) Chelkowski, A. *Dielectric Physics*; Elsevier: North-Holland, NY,1980.

DOI: 10.1021/acs.jced.5b00131
J. Chem. Eng. Data 2015, 60, 3093−3100

(14) Sliwinska-Bartkowiak, M.; Gras, J.; Sikorski, R.; Radhakrishnan, R.; Gelb, L.; Gubbins, K. E. Phase Transitions in Pores: Experimental and Simulation Studies of Melting and Freezing. *Langmuir* **1999**, *15*, 6060−6069.
(15) Kaneko, K.; Watanabe, A.; Iiyama, T.; Radhakrishnan, R.; Gubbins, K. E. A remarkable elevation of freezing temperature of CCl_4 in graphitic micropores. *J. Phys. Chem. B* **1999**, *103*, 7061−7063.
(16) Sliwinska-Bartkowiak, M.; Jazdzewska, M.; Gubbins, K. E.; Huang, L. Melting Behavior of Water in Cylindrical Pores: Carbon Nanotubes and Silica Glasses. *Phys. Chem. Chem. Phys.* **2008**, *10*, 4909−4919.
(17) Radhakrishnan, R.; Gubbins, K. E.; Watanabe, A.; Kaneko, K. Freezing of simple fluids in microporous activated carbon fibers: Comparison of simulation and experiment. *J. Chem. Phys.* **1999**, *111*, 9058−9067.
(18) Ayappa, K. G.; Mishra, R. K. Freezing of fluids confined between mica surfaces. *J. Phys. Chem. B* **2007**, *111*, 14299−14310.

DOI: 10.1021/acs.jced.5b00131
J. Chem. Eng. Data 2015, 60, 3093−3100